

Journal of Materials Chemistry C

Accepted Manuscript



This is an *Accepted Manuscript*, which has been through the Royal Society of Chemistry peer review process and has been accepted for publication.

Accepted Manuscripts are published online shortly after acceptance, before technical editing, formatting and proof reading. Using this free service, authors can make their results available to the community, in citable form, before we publish the edited article. We will replace this *Accepted Manuscript* with the edited and formatted *Advance Article* as soon as it is available.

You can find more information about *Accepted Manuscripts* in the [Information for Authors](#).

Please note that technical editing may introduce minor changes to the text and/or graphics, which may alter content. The journal's standard [Terms & Conditions](#) and the [Ethical guidelines](#) still apply. In no event shall the Royal Society of Chemistry be held responsible for any errors or omissions in this *Accepted Manuscript* or any consequences arising from the use of any information it contains.



Graphene oxide -stimulated acoustic attenuating performance of Tungsten based Epoxy films†

Received 00th January 20xx,
Accepted 00th January 20xx

DOI: 10.1039/x0xx00000x

www.rsc.org/

Yunfeng Qiu,^{a‡} JingJing Liu,^{a‡} Huihui Yang,^a Feng Gao,^a Yue Lu,^a Rui Zhang,^{*b} Wenwu Cao,^{*b,c} PingAn Hu^{*a}

Tungsten/epoxy composite film integrated with graphene oxide (GO) is prepared via layer-by-layer assembly method, which shows enhanced acoustic attenuating performance compared with tungsten/epoxy composite film in the absence of GO. The basic structure consists of tungsten/epoxy/GO/epoxy (W/E/GO/E), in which the inner wrapped epoxy acts as a buffer layer to anchor GO nanosheets on W spheres, and the outer wrapped epoxy layer is designed to prevent GO nanosheets peeling off from W spheres. The designed structure was beneficial to guaranteeing the independence and integrity of the W/E/GO/E structure. The structure of the core-shell composites was characterized with Fourier-transform infrared spectra, Raman spectroscopy, Transmission electron microscope and X-ray photoelectron spectroscopy. The acoustic properties in the films were evaluated by a conventional pulse-echo overlap technique at the frequency of 9 MHz. It was found that the attenuation of the optimal W/E/GO/E composite films was much higher than those of traditional W films at a band frequency range from 5 MHz to 12 MHz, and 36.58 ± 0.2 dB/cm·MHz is obtained at 9 MHz. The wrapping of GO on the surface of W/E will create a crumpled surface for better mixing with epoxy matrix due to the hydrogen bonds and chemical bonds, leading to prepare high quality composite film with minimum structural defects including bubbles and cracks. The enhanced acoustic absorption property of the composite films was attributed to the synergistic effect among multicomponents, as well as the contribution of GO's thermoacoustic effect. The W/E/GO/E composite films with such excellent attenuation loss properties are promising to be the backing material for ultrasonic transducers.

Introduction

Tremendous efforts have been endeavoured into the development of backing materials for ultrasonic transducer with suitable acoustic impedance, high attenuation and robustness.¹⁻³ The acoustic impedance and the attenuation are two important parameters for backing materials. The former one can vary from 3 MRayl to 30 MRayl depending on the transducer design,⁴ and the latter one requires high value in all cases. Typically, backing materials are composed of a polymer matrix such as epoxy or polyurethane, and inorganic fillers of metallic particles including tungsten, iron, copper, magnesium and aluminium.⁵⁻⁷ Epoxy is often used as the polymer matrix in backing material⁸⁻¹¹ due to its good thermal stability,¹² environmental resistance,¹³ and mechanical properties.¹⁴ However, absorption of ultrasound in this kind of polymer is relatively low. To improve the attenuation property of the

epoxy composite, rubber modified² or surface modified epoxy¹⁵ were used to scatter the acoustic energy. Whereas, the different surface chemistry attribute of inorganic fillers and polymer matrix can cause high interfacial energy,¹⁶ leading to the structural defects including bubbles and cracks,¹⁷ thus showing deteriorated acoustic performance. Therefore, to develop a strategy to prepare high-quality composite film with minimum structural defects is a great breakthrough for obtaining high performance of backing materials.

GO consists of a hexagonal ring of carbon network having both sp² and sp³ hybridized carbon atoms bearing hydroxyl and epoxide functional groups on basal planes, as well as carbonyl and carboxyl groups at the edges of the sheet.¹⁸⁻²⁰ GO is considered to be hydrophilic due to its excellent dispersibility in water, and has also been found to possess amphiphilic properties with an edge-to-center distribution of hydrophilic and hydrophobic domains.^{21, 22} It is expected that the amphiphathy and flexibility of GO, and hydrogen bonding interaction between GO and epoxy might facilitate the co-assembly with W and epoxy. It has been proved that the electronic structure and chemical properties of GO can be altered by introducing functional groups, enabling them utilized in sensors,²³ fuel cells,²⁴ field-effect transistor devices,²⁵ bioscience and biotechnologies,²⁶ electromagnetic interference (EMI) shielding.²⁷ Recently, considerable efforts have been endeavoured to the development of graphene-based composites for novel microwave absorption materials owing to the improving dielectric constant, dispersion and

^a Key Lab of Microsystem and Microstructure, Harbin Institute of Technology, Ministry of Education, No. 2 Yikuang Street, Harbin, 150080, P.R. China

^b Condensed Matter Science and Technology Institute, Harbin Institute of Technology, Harbin 150080, China

^c Department of Mathematics and Materials Research Institute, The Pennsylvania State University, University Park, Pennsylvania 16802, USA

† Electronic Supplementary Information (ESI) available: [AFM image and photograph; Scheme of hydrogen bonds and chemical bonds; Failure stress and strain, impedance, and attenuation of films; Thermogravimetric curves; Stress-strain curves; The pulse-echo immersion technique.]. See DOI: 10.1039/x0xx00000x

‡ Qiu. Y. and Liu. J. contributed equally to this work.

loss.^{28, 29} Meanwhile, GO-based thermoacoustic devices have already shown promising applications in the acoustic field due to the combination of exceptional electrical transport and thermal properties.³⁰⁻³² However, to the best of our knowledge there are no reports on the application of graphene composites as backing materials to absorb ultrasonic wave for ultrasonic transducer.

Herein, we report a reliable method for synthesizing high-quality W/E/GO/E composite films, in which GO was not only serving as the intermediate substance to solve fillers dispersion problem but also plays a major role in sound wave absorption. The LBL structure of W/E/GO/E was characterized in details. Acoustic impedance and attenuation loss of the films have been measured by a conventional pulse-echo overlap technique at a frequency of 9 MHz. The synergistic effect between W spheres and GO sheets would enhance their sound wave absorption properties. We believe the designed W/E/GO/E composite films with such excellent attenuation properties can provide new clues for preparing promising backing material for ultrasonic transducer.

Experimental

Materials

GO was synthesized via a modified Hummer method.^{26, 33} The commercial epoxy resin (T31) and hardener (W93) were supplied by Aladdin Reagent Company. A stoichiometric resin/hardening ratio 3:1 by weight was used according to the manufacturer's data sheets. Tungsten powders with particle size 12 μm (99.99%, Aladdin) were used as reinforcing and attenuation scattering agent.

Preparation of W/E/GO/E composite films

Typically, to fabricate a film with a basic structure of fillers consisting of 60 wt% W/3 wt% E/3.5 wt% GO/0.1 wt% E and 33.5% epoxy resin as polymer matrix, 12 μm tungsten powders were firstly dispersed with diluted epoxy resin ethanol solution. Afterwards, the mixture was stirred and dried for 1 h at 45 °C to obtain the tungsten/epoxy (W/E) particles with W:E weight ratio of 60:3. Addition of epoxy decorated W spheres into a 100 ml GO aqueous solution (weight ratio for W:GO was 60:3.5), the mixture was ultrasonicated for 0.5 h. The as-prepared tungsten/epoxy/graphene oxide (W/E/GO) mixture was poured into a petri dish followed by drying at 45 °C for 12 h and then the dried mixture was grinded and filtered by a 400 mesh sieve. Following, the W/E/GO composite particles were coated with an ultrathin layer of epoxy in the same way. 0.1 wt% was used to represent the content of the outer epoxy layer of W/E/GO/E composite. Similar to the former procedure, the ultimate W/E/GO/E composite particles were prepared by a 400 mesh sieve. Finally, W/E/GO/E composite particles and epoxy resin matrix were mixed according to the mass proportion of 66.5:33.5. The W/E/GO/E composite film was solidified in 4 h and polished to 2 mm thickness. The other films with different ratios were fabricated in the similar way.

Characterization

The morphology of the spheres was investigated by Scanning Electron Microscope (SEM) (SU800, Hitachi, 15 kV) and Transmission Electron Microscope (TEM) (G-20, FEI-Tecna, 100 kV). Raman spectra were obtained using a Horiba Xplore Raman system with 532 nm excitation. Fourier transform infrared (FTIR) measurements were performed in air using a Bruker FTIR spectrometer. Thermogravimetric analysis (TGA) were carried out using a thermal gravimetric analysis instrument (Shimadzu TGA-50H) with a flow rate of 20.0 mL min⁻¹ and a heating rate of 15 °C min⁻¹. X-ray photoelectron spectra (XPS) were measured using a Thermo Scientific X-ray photoelectron spectrometer (K-Alpha, Thermo Scientific, Waltham, MA, USA). The stress-strain experiments were carried out in a single-column testing instrument in tensile mode (Agilent Technologies T150UTM). The specimen was cut into dumbbell shape (inset (II) in Fig. S3), the two ends of the specimen were fixed on a stage. All tensile tests were conducted in a controlled force mode with a force ramp rate of 100 mN/min.

Ultrasonic absorption measurement

The ultrasonic measurements were performed using two immersion-type broadband ultrasonic transducers (Panamatrix V358; Parametric, Waltham, MA) with a central frequency of 9 MHz. The sample was sandwiched between the two immersed transducers, and then the velocity and attenuation are derived from the difference of flight and amplitude between the sample and water.³⁴ The attenuation is calculated by taking the transmission coefficients into account at the water-sample and sample-water interfaces,³⁵ and the acoustic impedance of the sample was obtained by the product of the velocity and density.³⁶ The density of each sample was calculated by using the measured weight and volume, with the volume determined by the Archimedes method.

Results and discussion

Synthesis process of W/E/GO/E composite films

The fabrication process of LBL assembly W/E/GO/E film is described in Fig. 1. W/E spheres were synthesized by a simple coating procedure. Thin epoxy layer solidified on W surface and the shrinkage characteristic of epoxy during the curing process is beneficial to the encapsulation of epoxy on W surface,³⁷ resulting in W/E core-shell structure. Then, W/E sphere was assembled by GO sheet and an ultrathin epoxy layer by layer, a triple layer structure of W/E/GO/E sphere was obtained. Fig. S1a in Supporting Information shows few-layer GO sheet, and stable dispersion solution of W/E spheres was formed in the presence of high GO concentration (Fig. S1c). Figure S1b shows the metastable aqueous solutions of pure GO and the mixture of GO and W/E spheres. The composite solution was dried and crushed into powder, W/E/GO with LBL structure was obtained after filtering through a 400 mesh sieve. Seen in Fig. S1d, final spheres of W/E/GO/E composite were prepared according to similar epoxy coating strategy. After

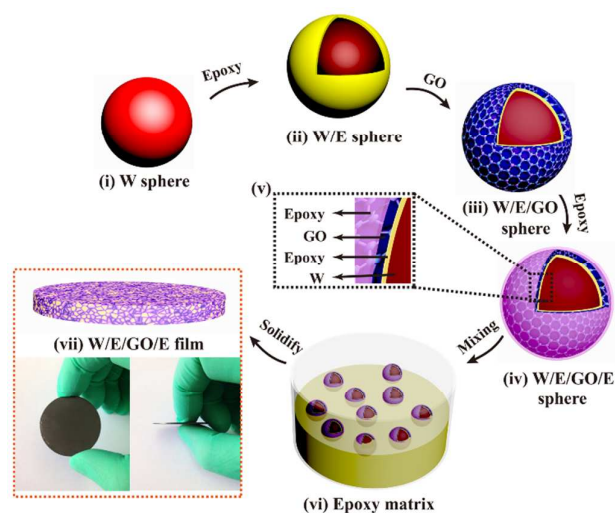


Fig. 1 Schematic fabrication process of W/E/GO/E film. (i) Naked W spheres with average diameter of 12 μm , (ii) W/E sphere was fabricated by coating ~ 50 nm epoxy on W sphere, (iii) W/E/GO and (iv) W/E/GO/E spheres were prepared in the similar way, respectively. (v) The LBL structure of W/E/GO/E. (vi) Dispersion of W/E/GO/E powders in epoxy solution by stirring. (vii) Final W/E/GO/E film with ~ 2 mm thickness processed by solidification and polish.

mixing W/E/GO/E spheres and epoxy matrix, and subsequent solidification and polish, a 2 mm thickness composite film was fabricated. Fig. S1f shows the optical image of film with smooth and homogeneous surface. Several advantages are expected from as-fabricated core-shell structure. First, the inner epoxy layer acted as a buffer layer that facilitated GO sheets to adhere on W surface firmly. GO and epoxy had similar wettability, and the hydroxyl and epoxide functional groups of GO will form multi-hydrogen bonds with functional residues of epoxy resin.³⁸ Second, the shrinkage occurs when epoxy layer solidified on W surface, excluding cavities between W spheres and epoxy matrix. This structure is beneficial to facilitating sound wave penetrating into GO network structure. It is assumed that sound was absorbed by the impedance transmittance of the inner layer epoxy and the synergistic effect between W, epoxy and GO.³⁹ As a result, the designed composite films consisting of tungsten spheres with LBL structure as fillers might be expected to exhibit high uniformity, superior mechanical property and sound wave absorption ability.

Characterization of W/E/GO/E composite films

Fig. 2a and 2e shows the SEM and TEM images of W spheres with an average diameter of 12 μm , in which W particles had smooth and clean surface. As seen in Fig. 2b, W/E composite spheres were obtained by evenly assembling epoxy on W spheres. TEM image in Fig. 2f illustrate that the interfaces of W sphere and epoxy layer was clear and the thickness of epoxy layer was about 50 nm. Seen in SEM image of Fig. 2c, GO nanosheets were attached to the W/E surface closely because of the non-covalent interactions between the hydroxyl and epoxide functional groups of GO and the functional residues of epoxy resin.³⁸ Wrinkles of GO on W/E/GO surface were obviously observed. Fig. 2g presents the TEM image of the

interface state of W/E/GO structure, the selected section was amplified in Fig. 2h. W sphere, the inner coated epoxy layer and the outer coated GO layer were distinguished easily due to different electron penetrability. There are no cavities in W/Epoxy and Epoxy/GO interface, indicating that the intermediate epoxy layer is beneficial to eliminate bubbles in W/E/GO structure. Using selected area electron diffraction (SAED) pattern to verify the two layer material, two regions were labeled near the boundary of W/E/GO in Fig. 2h. Fig. 2i reveals the amorphous nature of epoxy resin, whereas Fig. 2j shows the polycrystalline phase of GO sheets.

The G-mode frequency (ω_G) Raman map of a W/E/GO particle in Fig. 2d clearly exhibits the even distribution of GO on W surface. The inset of Fig. 2d is the Raman spectra of the composite spheres, in which G band near 1595 cm^{-1} indicates sp^2 hybridization of carbon network and D band near 1350 cm^{-1} shows the defects in the GO's structure.⁴⁰ The characteristic Raman G peak at around 1580 cm^{-1} in W/E/GO/E (magenta line, Fig. 3a) is obviously broadened and blue-shifted relative to that of GO (blue line, Fig. 3a), indicating lower disorder of GO in epoxy matrix.⁴¹ In addition, a universal observation from previous work is that higher disorder in graphite causes a broader G band D band, and higher ID/IG ratio.⁴¹ It is found that the intensity ratio of D and G peaks decreases slightly from 0.98 to 0.90 in W/E/GO/E composite comparing to that of GO. This change reflects the lower structure disorder in W/E/GO/E composite,⁴¹ indicative of GO functional groups were bounded by epoxy functional groups. The W/E/GO/E composite also shows the characteristic peaks of pure epoxy (red line, Fig. 3a), proving the existence of GO and epoxy in the composite.

To further elucidate the interaction force between epoxy layer and GO layer in W/E/GO/E composite, FTIR spectroscopy was employed to measure functional groups in the composite materials. Fig. 3b shows the FTIR spectra of W, Epoxy, GO and W/E/GO/E powders, respectively. W/E/GO/E were fabricated in different loading amounts of the GO and abbreviated as W/E/GO/E (I) and W/E/GO/E (II). The band at 1725 cm^{-1} in W/E/GO/E composite is about 7 cm^{-1} blue-shifted relative to

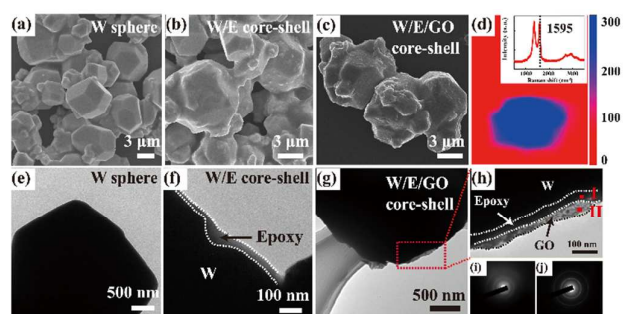


Fig. 2 Characterization of W spheres, W/E and W/E/GO core-shell structures. SEM (a) and TEM (e) images of W spheres. SEM (b) and TEM (f) images of W/E core-shell particles, the two white dotted lines in (f) indicate the profile of epoxy layer. SEM (c) and TEM (g, h) images of W/E/GO particles at low and high magnifications; Outer layer of GO and inner layer of epoxy are labeled in (h). (d) The ω_G Raman map of a W/E/GO sphere, inset is the corresponding Raman spectra. (i) and (j) are SAED patterns for positions labeled as I and II in (h), respectively.

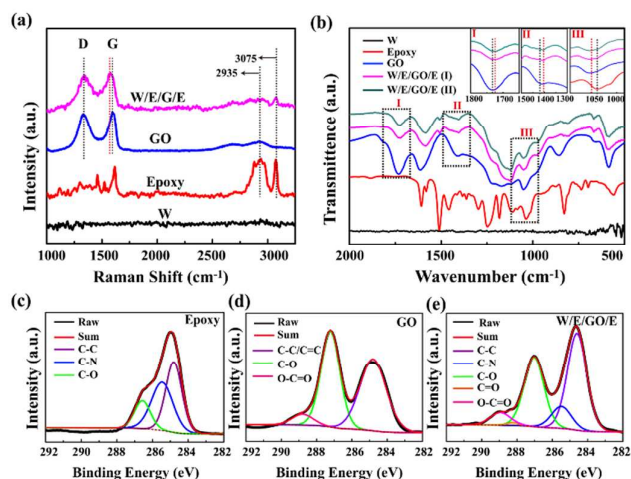


Fig. 3 (a, b) Raman and FTIR spectra of W, epoxy, GO and W/E/GO/E spheres. The insets of (b) were the magnified regions of the rectangle boxes. (c) XPS spectra of epoxy, (d) GO sheets and (e) W/E/GO/E composite spheres.

that at around 1732 cm^{-1} in pure GO (inset I in Fig. 3b), attributing to the formation of hydrogen bonds between -COOH in GO and epoxy groups in epoxy resin.⁴² This interaction made the stretching vibration of carboxyl acid more localized.⁴³ The decreasing intensity of this band for W/E/GO/E composite also indicated the decreasing carboxyl acid stretching modes comparing to pure GO. In addition, a significant blue-shift between 1409 cm^{-1} band in pure GO and 1403 cm^{-1} band in W/E/GO/E composite (inset II in Fig. 3b) is assigned to the deformation vibration mode of O-H existed in -COOH or carbon skeleton. It is also found that there was about 10 cm^{-1} red-shift owing to the C-O stretching vibration among 1035 cm^{-1} in pure epoxy and 1045 cm^{-1} in W/E/GO/E composite in Fig. 3b (III). In addition, the 1614 cm^{-1} band located in pure GO and 1583 cm^{-1} band appeared in W/E/GO/E composites were assigned to the stretching and bending vibration of -OH groups of water molecules adsorbed on GO and W/E/GO/E composites. The absorption peaks at 1120 cm^{-1} both in GO and W/E/GO/E is corresponding to the stretching vibration of C-OH. Additionally, besides the hydrogen bonds between GO and epoxy deduced from FTIR analysis, there also might exist chemical reaction between epoxides from epoxy with nucleophiles like -COOH in GO⁴⁴. As proved in many papers, epoxide can react with -COOH to form ester bonds. Scheme S1 showed the possible hydrogen bonds and chemical bonds between the epoxy resin and GO.

The chemical structure of W/E/GO/E composite and the interaction between epoxy and GO was further investigated by XPS. Fig. 3c to Fig. 3e shows the C 1s core-level spectra of pristine epoxy (Fig. 3c), pristine GO (Fig. 3d), and W/E/GO/E composite (Fig. 3e), respectively. The C 1s core-level spectrum of the pristine epoxy could be deconvoluted into three peaks with binding energies at 284.8 eV for C-C species, 285.6 eV for C-N species and 286.5 eV for C-O species, respectively.⁴⁵ In pristine GO, binding energies at 288.9 eV for O=C-O species appeared, and the higher C-O peak indicates that GO has a high degree of oxidative functional groups.⁴⁶ For the

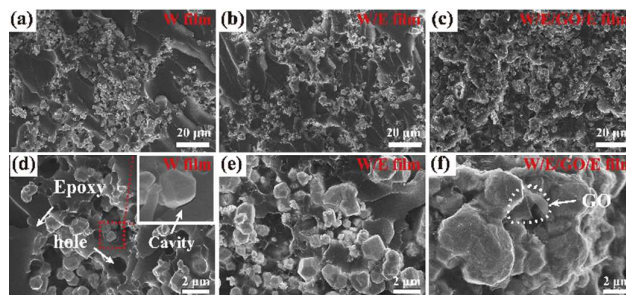


Fig. 4 (a, d) The cross-sectional SEM images of W film, (b, e) W/E film, (c, f) W/E/GO/E film in low and high magnifications. The inset of (d) was the enlarged region of red square showing the gap between W sphere and epoxy matrix.

W/E/GO/E composite, it maintains C-C, C-N, C-O, and O=C-O bonds in epoxy and GO, indicating the presence of epoxy layer and GO layer on the surface of W sphere. Meanwhile, the additional peak of C=O species appears in W/E/GO/E suggesting that the hydrogen bond generating from -COOH in GO and oxygen-containing or nitrogen-containing groups in epoxy resin. TGA of W, epoxy, GO and W/E/GO/E composite materials were carried out under N_2 flow from room temperature to $800\text{ }^\circ\text{C}$ at $15\text{ }^\circ\text{C}/\text{min}$. The results are shown in Fig. S2. As expected, W was highly stable up to $800\text{ }^\circ\text{C}$. Epoxy and GO both show significant mass decrease from $60\text{ }^\circ\text{C}$ to $650\text{ }^\circ\text{C}$. The major mass reduction at $\sim 150\text{ }^\circ\text{C}$ was caused by pyrolysis of the oxygen-containing functional groups, generating CO, CO_2 and steam.⁴⁷ W/E/GO/E composites were marked as (a), (b) and (c) corresponding to different mass ratio of W:E:GO:E, the mass loss details were shown in Table S1.

The homogeneous structure of composite film was confirmed by the cross-sectional SEM images of Fig. 4. Fig. 4a shows the cross-sectional SEM image of 60 wt% W spheres dispersed in 40 wt% epoxy matrix. It can be found that W spheres were aggregated in epoxy, attributing to the poor miscibility of metal W spheres in epoxy during the stirring process.⁴⁸ The mismatch of the interfacial energy between W spheres and epoxy matrix leads to the negative structural issues, confirmed in Fig. 4d, thus cavities appeared at the interface of W sphere and epoxy matrix (inset, Fig. 4d). The W film possesses weak mechanical behaviour, in which W spheres can be separated from the epoxy matrix easily when break off the film, leaving many holes at fracture surface (Fig. 4d). This problem was improved substantially when W spheres were decorated by a buffer layer of epoxy, making W spheres stayed at the fracture surface (W/E film, Fig. 4b and 4e). Epoxy buffer layer reduced cavities at the interface between fillers and polymer matrix. The stronger adhesion stress of W/E films compared to W films was also verified by the stress-strain curve in Fig. S3, in which the failure stress of W/E film was higher than that of W film.

The homogeneity of W/E film (Fig. 4b) was improved slightly comparing to that of W film (Fig. 4a). W/E composite spheres were further modified by GO and an ultrathin epoxy, then being filled in the epoxy matrix to get the W/E/GO/E film. From Fig. 4c we can see W/E/GO/E spheres (60 wt% W) were dispersed in epoxy matrix uniformly. W/E spheres were completely wrapped by graphene sheets, and the wrinkles of

GO sheets can be observed easily (Fig. 4f). The high quality film without bubbles and cavities was of great importance to improve the film's acoustic performance. Although the stress of W/E/GO/E film was lower than those of W/E film and W film, it exhibited the best bendability. As shown in Fig. S3, the failure strain of W/E/GO/E composite films was up to 8.5 %, which was much larger than those W films and W/E films. It can be bended to 60° without any damage, and also recovers to original state after removing the force. In the case of W/E/GO/E spheres (60 wt% W) composites, the cross-linking degree of epoxy may be decreased when compared with those of W/E composites, which thus produced the flexibility of the composites. As reported in previous work, the failure stress of graphene/epoxy composites is highly dependent on the interfacial debonding between graphene and epoxy matrix.⁴⁹ The good dispersion of W and GO is attributed to the coating layer of epoxy on their surface. In Tang's work, both the good dispersion of GO and high quality interface ascribable to the incorporation of polyetheramine or diglycidyl ether of bisphenol on GO, contributed to the high failure stress of composite film. Present W/E/GO/E spheres may not be an ideal filler for the enhancement of mechanical performance, due to the weak interfacial interaction between GO and epoxy. Additionally, the cross-linking degree of epoxy may be decreased when integration with those fillers, leading to the lower failure stress of W/E/GO/E film.

Sound absorption properties of W/E/GO/E composite films

To test the applicability of epoxy composites as backing material, the acoustic impedance and attenuation of the W/E/GO/E composite films were measured by a pulse-echo immersion technique² (Fig. S4a). Samples were sandwiched between two immersed transducers with a distance of 10 cm. The structure of W/E/GO/E composite film designed to be the promising candidate for the ultrasonic baking absorber material was analysed in details.

First, we compare the acoustic impedance (Fig. 5a) and attenuation (Fig. 5b) of films fabricated by W spheres and W/E spheres with the W content from 20 to 80 wt%. In Fig. 5a, the considerable increasing in acoustic impedance with the increasing W content was observed, ascribing to the improved cross-linking density and the multiple reflection between W fillers and polymer interfaces.¹⁵ It can be explained by the following equation:

$$Z = \rho V \quad (1)$$

Where, Z , V and ρ were the acoustic impedance, velocity and density, respectively.³⁶ W/E films had a higher acoustic impedance value compared to W films, ascribing to the closer packed structure of W/E films than that of W films (Fig. 4d and 4e). The attenuation peaks of W and W/E films were both obtained around 60 wt% tungsten, which was also reported in previous work.⁵¹ The structure with cavities at the interface of W particles and epoxy matrix in W films increased the acoustic scattering and multi-reflecting of ultrasonic waves in W spheres because W and air had a wide difference in impedance. W films had greater attenuation loss than W/E films (Fig. 4b).

To research the influence of the acoustic performances by the different content of GO, the GO/E and W/GO/E films were studied (Fig. 5c and Fig. 5d). Fig. S4b shows direct mixing GO powder and epoxy matrix to fabricate the GO film, the poor dispersibility of GO (inset Fig. S4b) result the instability of the acoustic performance of the GO film. When GO was modified with a thin epoxy layer (0.1 wt%), the problem was solved. Fig. 5c and Fig. 5d show the highest peak attenuation value at 3.5 wt% GO in GO/E and W/GO/E films. In Fig. 5c, the film also has a relatively good attenuation value as GO content was improved to 8 wt%. Considering the costs, we choose 3.5 wt% to be the best GO loading level. The attenuation of W/GO/E films is larger than the sum of the attenuation of W and GO/E films, illustrating that a synergistic effect occurred between W and GO. The acoustic impedance of W/GO/E films was stable in 5-7 MRayl with the increasing GO content. At last, to discuss the influence of the epoxy buffer layer of the ultimate structure of W/E/GO/E, different content of inner layer epoxy W/E/GO/E films were fabricated. Fig. 5e shows the attenuation value increased with increasing epoxy buffer layer contents and the optimal attenuation loss 36.58±0.2 dB/cm-MHz was obtained at 5 wt% epoxy layer.

Fig. 6a is the comparison of attenuation performance of optimized W/E/GO/E film (60 wt% W, 5 wt% E, 3.5 wt% GO, 0.1 wt% E), W/GO/E (60 wt% W/3.5 wt% GO/0.1 wt% E) film, W/E (60 wt% W/5 wt% E) film, and conventional W film at the band frequency ranging from 5 MHz to 12 MHz. It is found that the attenuation loss of W/E/GO/E film is much larger than W/GO/E film without inner epoxy layer on the surface of W spheres, W/E film without GO, and naked W film, confirming the great importance of the introduction of inner epoxy layer and GO. Fig. 6b shows the three-dimensional presentation of calculated theoretical absorption coefficients of this W/E/GO/E composite film at various thicknesses (1-10 mm) in the frequency range of 2-20 MHz. It indicates that the ultrasonic wave absorbing ability of W/E/GO/E film at different frequencies can be adjusted by controlling the thickness of the absorbents. When the film was 1 mm, its absorption coefficient would reach 90% at 12 MHz. Meanwhile, the absorption coefficient would reach 90 % as the film is thicker than 5 mm at the frequency of 2 MHz. Under the experiment conditions of 9 MHz frequency and 2 mm thickness, the absorption coefficient reaches 96.98%, indicating that the composite film can act as an outstanding backing absorber.

For comparison, we summarized the attenuation values of our work and previously reported metallic fillers/polymer at 5 MHz in Fig. 6c. Generally, for our LBL assembled W/E/GO/E film, the attenuation loss (175 dB/cm) is about two to five times higher than those of W/polymer composites^{2, 4, 52, 53} (34-90 dB/cm) and is obviously higher than Al₂O₃/PU⁵⁴ (85.6 dB/cm), Ti/Si/epoxy¹⁵ (50.34 dB/cm) and W/Al₂O₃/polymer films⁵⁴ (154.2 dB/cm). The outstanding burnable polymeric composite (W (Burps)/spurr epoxy) (217 dB/cm) was fabricated by a series of complex mixing and 1100 °C sintering process⁴. Such sophisticated preparation process will somehow hinder the development of practical application of backing materials. By

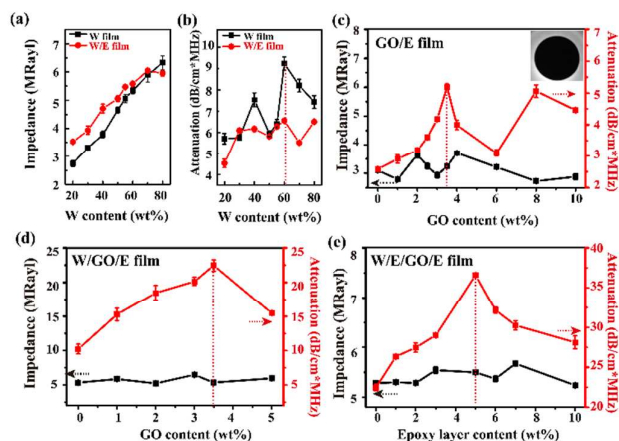


Fig. 5 (a, b) The acoustic impedance and attenuation values of W and W/E composite films versus tungsten contents, respectively. (c, d) The acoustic impedance and attenuation values on GO contents for GO/E films and W/GO/E films. The inset of (c) is the photograph of a GO/E film. (e) The acoustic impedance and attenuation values versus the inner epoxy content for W/E/GO/E films.

comparison, our LBL method for the preparation of backing materials is more convenient and controllable.

The enhanced acoustic effects were determined by the film structure, we propose a schematic illustration of the sound wave absorption mechanism based on the microstructure characteristics of the epoxy and GO wrapped W spheres, as shown in Fig. 7. When W spheres were directly filled in the epoxy matrix, there were cavities at the interfaces between W and epoxy (seen in Fig. 4d), which were caused by interfacial energy mismatching. The incident sound wave undergoes multiple reflections and absorption inside the W sphere, because the air with low impedance prevents sound wave

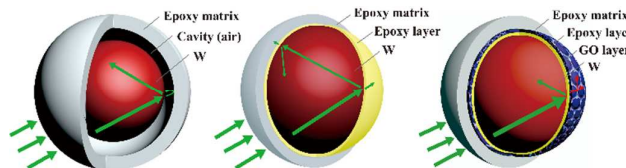


Fig. 7 A schematic illustration of ultrasonic wave absorption modes in W (a), W/E (b), and W/E/GO/E films (c).

from transmitting into epoxy matrix.⁵⁵ Whereas W spheres were wrapped by a thin layer epoxy to exclude the cavities during the curing shrinkage process of the epoxy layer and the adhesion between epoxy layer and epoxy matrix.³⁷ The epoxy layer acted as the impedance transition layer to guide the waves propagating into epoxy matrix, decreasing the sound absorption properties (shown in Fig. 5b). GO sheets were further coated on the W/E spheres surfaces, leading to the possibility that the transmitted sound waves could propagate into GO sheets due to the similar approaching impedance (GO 2.71 MRayl,⁵⁶ epoxy 3.05 MRayl⁵⁷) of GO and epoxy layer. Sound waves spreading on GO surface were quickly transformed into thermal energy due to the thermoacoustic effect of GO, in which sound wave and Joule heating could transform into each other,^{31, 58} thus enhanced the absorption attenuation by the synergistic effect of W, epoxy and GO.

Conclusions

W/E/GO/E composite spheres have been successfully synthesized via a LBL assembly process of epoxy layer and GO sheets on W spheres. The hybrids in the epoxy matrix exhibit better uniformity and enhanced ultrasonic absorption properties. The improved film quality was mainly ascribed to hydrogen bonds and chemical bonds between GO and epoxy layer, which greatly decreased the structural defects. The maximum attenuation loss reaches 36.58 ± 0.2 dB/cm·MHz at 9 MHz, and the absorption coefficient reaches 96.98 % for 2 mm sample. The enhanced acoustic performance was determined by the modulation of sound waves spreading pattern, viz the sound waves spreading on GO surface were quickly transformed into thermal energy due to the thermoacoustic effect of GO in W/E/GO/E composite film. The outstanding absorption property was promoted by the synergistic effect of W, epoxy and GO sheets. Our study provides a promising strategy to fabricate backing materials for ultrasonic transducer with high attenuation and moderate impedance.

Acknowledgements

This work is supported by the National key Basic Research Program of China (973 Program) under Grant No. 2013CB632900, the National Natural Science Foundation of China (NSFC, No.61172001, 21373068, 21303030),

Notes and references

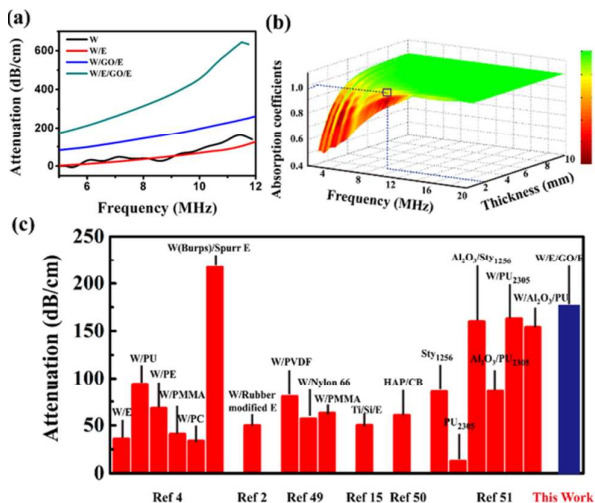


Fig. 6 (a) The comparison of attenuation values of W/E/GO/E (60 wt% W/5 wt% E/3.5 wt% GO/0.1 wt% E) film, W/GO/E (60 wt% W/3.5 wt% GO/0.1 wt% E) film, W/E (60 wt% W/5 wt% E) film, and W film (60 wt%) at a band frequency ranging from 5 to 12 MHz. (b) Three-dimensional presentation of the absorption coefficient of the composite films with different thickness in the frequency range of 2.0–20.0 MHz. (c) Comparison of our W/E/GO/E films with the reported metallic fillers/polymer film at the frequency of 5 MHz.

- 1 M. Toda and M. Thompson, *IEEE T. Ultrason. Ferr.*, 2012, **59**, 231-242.
- 2 N. T. Nguyen, M. Lethiecq, B. Karlsson and F. Patat, *Ultrasonics*, 1996, **34**, 669-675.
- 3 K. R. Chapagain and A. Ronnekleiv, *IEEE T. Ultrason. Ferr.*, 2013, **60**, 2440-2452.
- 4 M. G. Grewe, T. R. Gururaja, T. R. Shrout and R. E. Newnham, *IEEE T. Ultrason. Ferr.*, 1990, **37**, 506-514.
- 5 R. Zhang, W. Cao, Q. Zhou, J. H. Cha, K. K. Shung and Y. Huang, *IEEE T. Ultrason. Ferr.*, 2007, **54**, 467-469.
- 6 K. Sugawara, M. Nishihira and K. Imano, *Japanese Journal of Applied Physics Part 1-Regular Papers Brief Communications & Review Papers*, 2005, **44**, 4347-4349.
- 7 S. K. Jain, R. Gupta and S. Chandra, *Ultrasonics*, 1998, **36**, 37-40.
- 8 K. J. Kirk and N. Schmarje, *Ultrasonics*, 2013, **53**, 185-190.
- 9 L. Yuli, C. Gin-Shin, L. Hsin-Chih and L. Yu-Cheng, *Adv. Mater. Res.*, 2012, **476-478**, 2105-2108.
- 10 F. Tiefensee, C. Becker-Willinger, G. Heppel, P. Herbeck-Engel and A. Jakob, *Ultrasonics*, 2010, **50**, 363-366.
- 11 F. Lionetto and A. Maffezzoli, *Adv. Polym. Technol.*, 2008, **27**, 63-73.
- 12 M. A. Downey and L. T. Drzal, *Polymer*, 2014, **55**, 6658-6663.
- 13 T. Liu, Y. Nie, L. Zhang, R. Chen, Y. Meng and X. Li, *RSC Adv.*, 2015, **5**, 3408-3416.
- 14 L. Pan, S. Lu, X. Xiao, Z. He, C. Zeng, J. Gao and J. Yu, *RSC Adv.*, 2015, **5**, 3177-3186.
- 15 F. El-Tantawy and Y. K. Sung, *Mater. Lett.*, 2004, **58**, 154-158.
- 16 F. Hussain, M. Hojjati, M. Okamoto and R. E. Gorga, *J. Compos. Mater.*, 2006, **40**, 1511-1575.
- 17 B. Audoly, *J. Mech. and Phys. Solids*, 2000, **48**, 1851-1864.
- 18 P. Songfeng and C. Hui-Ming, *Carbon*, 2012, **50**, 3210-3228.
- 19 Y. Zhu, S. Murali, W. Cai, X. Li, J. W. Suk, J. R. Potts and R. S. Ruoff, *Adv. Mater.*, 2010, **22**, 3906-3924.
- 20 D. C. Marcano, D. V. Kosynkin, J. M. Berlin, A. Sinitskii, Z. Sun, A. Slesarev, L. B. Alemany, W. Lu and J. M. Tour, *ACS Nano*, 2010, **4**, 4806-4814.
- 21 N. D. Tissera, R. N. Wijesena, J. R. Perera, K. M. N. de Silva and G. A. J. Amaratunge, *Appl. Surf. Sci.*, 2015, **324**, 455-463.
- 22 L. J. Cote, J. Kim, V. C. Tung, J. Luo, F. Kim and J. Huang, *Pure Appl. Chem.*, 2011, **83**, 95-110.
- 23 F. Schedin, A. K. Geim, S. V. Morozov, E. W. Hill, P. Blake, M. I. Katsnelson and K. S. Novoselov, *Nat. Mater.*, 2007, **6**, 652-655.
- 24 X. Sun, J. P. He, J. Tang, T. Wang, Y. X. Guo, H. R. Xue, G. X. Li and Y. O. Ma, *J. Mater. Chem.*, 2012, **22**, 10900-10910.
- 25 C. A. Di, D. C. Wei, G. Yu, Y. Q. Liu, Y. L. Guo and D. B. Zhu, *Adv. Mater.*, 2008, **20**, 3289.
- 26 Z. Liu, J. T. Robinson, X. M. Sun and H. J. Dai, *J. Am. Chem. Soc.*, 2008, **130**, 10876-10882.
- 27 J. J. Liang, Y. Wang, Y. Huang, Y. F. Ma, Z. F. Liu, F. M. Cai, C. D. Zhang, H. J. Gao and Y. S. Chen, *Carbon*, 2009, **47**, 922-925.
- 28 C. Wang, X. J. Han, P. Xu, X. L. Zhang, Y. C. Du, S. R. Hu, J. Y. Wang and X. H. Wang, *Appl. Phys. Lett.*, 2011, **98**, 072906.
- 29 L. N. Wang, X. L. Jia, Y. F. Li, F. Yang, L. Q. Zhang, L. P. Liu, X. Ren and H. T. Yang, *J. Mater. Chem. A*, 2014, **2**, 14940-14946.
- 30 H. Tian, D. Xie, Y. Yang, T.-L. Ren, Y.-F. Wang, C.-J. Zhou, P.-G. Peng, L.-G. Wang and L.-T. Liu, *Nanoscale*, 2012, **4**, 2272-2277.
- 31 H. Tian, T.-L. Ren, D. Xie, Y.-F. Wang, C.-J. Zhou, T.-T. Feng, D. Fu, Y. Yang, P.-G. Peng, L.-G. Wang and L.-T. Liu, *ACS Nano*, 2011, **5**, 4878-4885.
- 32 H. Tian, C. Li, M. A. Mohammad, Y.-L. Cui, W.-T. Mi, Y. Yang, D. Xie and T.-L. Ren, *ACS Nano*, 2014, **8**, 5883-5890.
- 33 G. Eda and M. Chhowalla, *Adv. Mater.*, 2010, **22**, 2392-2415.
- 34 L. A. E. B. Cobus, K. A. Ross, M. G. Scanlon and J. H. Page, *J. Agric. Food Chem.*, 2007, **55**, 8889-8895.
- 35 M. Treiber, J.-Y. Kim, L. J. Jacobs and J. Qu, *J. Acoust. Soc. Am.*, 2009, **125**, 2946-2953.
- 36 G.-J. Yao, Z.-W. Cui, R.-L. Song and K.-X. Wang, *J. Appl. Phys.*, 2007, **102**, 104903.
- 37 S. H. Hsu, R. S. Chen, Y. L. Chang, M. H. Chen, K. C. Cheng and W. F. Su, *Acta Biomater.*, 2012, **8**, 4151-4161.
- 38 S. L. Qiu, C. S. Wang, Y. T. Wang, C. G. Liu, X. Y. Chen, H. F. Xie, Y. A. Huang and R. S. Cheng, *Express Polym. Lett.*, 2011, **5**, 809-818.
- 39 T. E. G. Alvarez-Arenas, *IEEE T. Ultrason. Ferr.*, 2004, **51**, 624-633.
- 40 A. Kaniyoor and S. Ramaprabhu, *Aip Advances*, 2012, **2**.
- 41 K. N. Kudin, B. Ozbas, H. C. Schniepp, R. K. Prud'homme, I. A. Aksay and R. Car, *Nano Lett.*, 2008, **8**, 36-41.
- 42 T. Zhou, S. Nagao, T. Sugahara, H. Koga, M. Nogi, K. Suganuma, T. T. Nge and Y. Nishina, *RSC Adv.*, 2015, **5**, 20376-20385.
- 43 M. Cano, U. Khan, T. Sainsbury, A. O'Neill, Z. M. Wang, I. T. McGovern, W. K. Maser, A. M. Benito and J. N. Coleman, *Carbon*, 2013, **52**, 363-371.
- 44 B. Shen, W. Zhai, M. Tao, D. Lu and W. Zheng, *Composites Science and Technology*, 2013, **77**, 87-94.
- 45 R. N. Sa, Y. Yan, Z. H. Wei, L. Q. Zhang, W. C. Wang and M. Tian, *ACS Appl. Mater. Interfaces*, 2014, **6**, 21730-21738.
- 46 D. R. Dreyer, S. Park, C. W. Bielawski and R. S. Ruoff, *Chem. Soc. Rev.*, 2010, **39**, 228-240.
- 47 S. M. Khoshfetrat and M. A. Mehrgardi, *Analyst*, 2014, **139**, 5192-5199.
- 48 K. Kita-Tokarczyk, J. Grumelard, T. Haefele and W. Meier, *Polymer*, 2005, **46**, 3540-3563.
- 49 Y.-J. Wan, L.-C. Tang, L.-X. Gong, D. Yan, Y.-B. Li, L.-B. Wu, J.-X. Jiang and G.-Q. Lai, *Carbon*, 2014, **69**, 467-480.
- 50 L.-Z. Guan, Y.-J. Wan, L.-X. Gong, D. Yan, L.-C. Tang, L.-B. Wu, J.-X. Jiang and G.-Q. Lai, *J. Mater. Chem. A*, 2014, **2**, 15058-15069.
- 51 H. F. Wang, T. Ritter, W. W. Cao and K. K. Shung, *IEEE T. Ultrason. Ferr.*, 2001, **48**, 78-84.
- 52 P. E. Bloomfield, W. J. Lo and P. A. Lewin, *IEEE T. Ultrason. Ferr.*, 2000, **47**, 1397-1405.
- 53 F. El-Tantawy, N. A. Aal, A. A. El-Daly, A. M. Abdel-Daiem, A. Bakry and Y. K. Sung, *Mater. Lett.*, 2004, **58**, 3388-3394.
- 54 M. State, P. J. Brands and F. N. van de Vosse, *Ultrasonics*, 2010, **50**, 458-466.
- 55 M. M. Stechert, *Anesth. Analg.*, 2007, **105**, 895-895.
- 56 L. G. Delogu, G. Vidili, E. Venturelli, C. Menard-Moyon, M. A. Zoroddu, G. Pilo, P. Nicolussi, C. Ligios, D. Bedognetti, F. Sgarrella, R. Manetti and A. Bianco, *P. Natl. Acad. USA.*, 2012, **109**, 16612-16617.
- 57 H. R. Chabok, J. M. Cannata, H. H. Kim, J. A. Williams, J. Park and K. K. Shung, *IEEE T. Ultrason. Ferr.*, 2011, **58**, 206-214.
- 58 H. Tian, Y. Yang, D. Xie, J. Ge and T.-L. Ren, *RSC Adv.*, 2013, **3**, 17672-17676.